Structure and chemistry investigations of Ni3InAs thin film on InAs substrate

Loïc Patout, Selma Rabhi, Carine Perrin-Pellegrino, Ahmed Charaï, Khalid Hoummada

Structure and chemistry investigations of Ni_3InAs thin film on InAs substrate

Loïc Patout, Selma Rabhi, Carine Perrin-Pellegrino,

Ahmed Charaï & Khalid Hoummada

IM2NP-CNRS, Aix-Marseille Université, Avenue Escadrille Normandie Niemen, Marseille, F-13397, France

Keywords

Thin film, Diffusive reaction, Intermetallic growth,

Self-aligned contacts, Epitaxy, Microstructure

Abstract

In situ X-Ray diffraction, Transmission Electron Microscopy (TEM) and Atom Probe Tomography (APT) were used to investigate the structure and the chemistry of the first phase formed after solid-state diffusive reaction between a Ni thin film (f) and an InAs substrate (s) at low temperature. The results show the formation of a single phase for which the Ni_3InAs stoichiometry and the $P6_3/mmc$-hexagonal (a = b = 4.00 Å and c = 5.10 Å) structure were evidenced. Investigations in Electron Diffraction are in agreement with a disordered $B8_{\sim 1.5}$ structure in which additional Ni atoms are randomly distributed with In and As on the equivalent interstitial sites. The epitaxy relationship was also found, namely the $[001]_s//[210]_f$ zone axes as well as the $(220)_s//(-120)_f$ and $(002)_s//(100)_f$ atomic planes. These findings were discussed taking into account atomic size effects.

1. Introduction

Nanoscale devices are reaching their limits for conventional silicon (Si) and metal-oxide semiconductor (CMOS) transistors so that new strategies have to be identified for the next generation. One of the major challenges is the development of Ohmic source/drain (S/D) contacts **[1-3]** to minimize the drain induced barrier lowering effects while low contact resistivities with Ohmic interfaces are suitable for reduced parasitic resistances **[4]**. Among the semiconductors, indium arsenide (InAs) has been identified as a particularly beneficial channel material for high performance transistors, as it offers high electron mobility and outstanding frequency response. It has been shown to have excellent on/off state switching properties as demonstrated in several experimental transistors **[5]**. Self-aligned contacts with metal silicides are usually prepared by a deposition followed by annealing. A similar routine may be essential for economical mass production of III-V based transistors with highly scaled dimensions. InAs n-FETs, in both thin film and nanowire channel configurations, have already been demonstrated to outperform conventional Si MOSFETs **[6-9]**. Ni has been employed as a component in a wide array of both Schottky and Ohmic metallization schemes in GaAs device technology **[10-12]**. It was recently shown that self-aligned silicide-like contacts can be made with InAs using Ni to form a ternary Ni_xInAs compound **[13]**. A first report of the formation of Ni_xInAs crystal and $Ni_xInAs/InAs/Ni_xInAs$ heterostructure nanowires by solid source reaction of InAs nanowires with Ni was described. The fundamental kinetic of the reaction was explored and the Ni diffusion was reported as the rate determining step **[14]**. Studies were done to understand the reactions between metals and semiconductors, the selection of thermally stable metallization materials **[15-18]**, as well as interfacial morphology in metal/GaAs contacts **[19]**. Theoretical and experimental methods were used to identify the crystal structure of the Ni-In-As ternary compounds, and study their mechanical and electronic properties **[13, 20]**. To date, little is known about structures and

stoichiometries. Some studies suggest Ni_3InAs or Ni_2InAs and also other different stoichiometries **[14, 21-22]**. Ingerly et al demonstrated the existence of a eutectic reaction occurring at 810 ± 5°C with the $Ni_{0.48}Ga_{0.30}As_{0.22}$ composition **[23]**. Metal/InAs alloys have been poorly explored with only limited information available in the literature. Therefore, developing and characterizing metal/InAs alloys with low resistivity and abrupt interfaces as the contact material to InAs is of major interest. Furthermore, since the texture, the phase sequence and especially the intermetallic film stability can be impacted by the deposited metal thickness **[24]**, the study of the intermetallic formation at reduced dimensions is needed.

Hence, in this work, we investigate the solid-state reaction between a Ni film of 100 nm thickness with an InAs substrate at low temperature using state-of-the-art characterization techniques. In situ X-Ray Diffraction (XRD) measurements have been carried out to characterize the texture and the sequence of phase formation. High Resolution Transmission Electron Microscopy (HRTEM) and Electron Diffraction (ED) experiments were carried out to identify the crystal structure (space group and lattice parameters) of the formed phase as well as the epitaxy relationship with the substrate. X-Ray Energy-Dispersive Spectrometry (EDS) and Atom Probe Tomography (APT) allowed to measure the stoichiometry and the homogeneity of the phase.

2. Experimental

A 100 nm thick Ni layer was deposited on an InAs (001) wafer using a 99.9999% pure Ar gas flow to sputter a 99.99% pure Ni target, in a commercial Von Ardenne CS730S magnetron sputtering system exhibiting a base pressure of 10^{-8} Torr at room temperature. The deposition was performed during sample rotation of 5 rpm in order to get a constant thickness. The InAs (001) substrate was cleaned with diluted nitric acid HNO_3 prior to the Ni deposition. To prevent the Ni/InAs nanostructure from atmospheric contamination, the sample was capped by a 20 nm thick TiN film in the same conditions as for the Ni deposition.

In situ measurements were carried out in order to follow the evolution of the formed phase after the solid-state reaction between the Ni metallic film and the InAs substrate. The as-deposited sample was mounted on an adapted furnace and then annealed under secondary vacuum at 175°C for 69 h on a two-circle X'Pert MPD diffractometer. The diffractometer is equipped with a copper anode tube (λ = 1.54 Å) operating at 40 kV and 40 mA. The result is given as an intensity color map (Fig. 1a). The X and Y axes carry the 2θ diffraction angle and the annealing time respectively.

After annealing, the microstructure of the formed phase was studied by TEM on cross-section and plan-view samples; their thicknesses were about 100 nm. The cross-section lamella was prepared by Focused gallium Ion Beam (FIB) milling using a Thermo Fisher dual beam HELIOS 600 nanolab setup. The standard lift-out technique was applied **[25]**. A Platinum (Pt) parallelepiped layer (1 µm height x 15 µm length x 2 µm width) was beforehand deposited on the TiN/Ni_3InAs film in order to delimit the area to be machined and to preserve the phase integrity underneath. The plan-view lamella was prepared differently: a mechanical polishing of the substrate down to few microns of thickness, followed by an argon ion milling down to few tens of nanometers using a GATAN Precision Ion Polishing System (PIPS-1). In this second step, two collimated Ar-beams milled the substrate face at the center of a sample area in rotation with energies ranging from 6 to 2 keV at low angle (5°).

HRTEM images were performed at 200 keV with a Field Emission Gun (FEG) Thermo Fisher Titan microscope equipped with a spherical aberration (Cs) correction system. In our recent studies concerning structure analyses of lanthanide tungstate phases, HRTEM images were calculated using Cs values of -0.03 mm **[26]** and -0.05 mm **[27]** that gave a good agreement with the experiments. We consider the Cs value in an order of magnitude between 0 and -0.05 mm allowing to reach a point-to-point resolution around 1Å. Energy Dispersive X-Ray Spectrometry (EDS) and electron diffraction (ED) analyses were acquired with a LaB_6

Thermo Fisher Tecnai TEM at 200 keV equipped with a silicon drift detector OXFORD X-max80. An EDS profile in multiple-point was used for a semi-quantitative analysis of the film. A probe size of about 10 nm allowed to obtain an output rate around 100 kcps processed by the system. The individual points were acquired every one nanometer with a clock time of 0.5 second. The dead time for processing the photons by the system was less than 20%. The profile was averaged on 10 successive acquisitions. The Cliff-Lorimer approach allowed to estimate the atomic composition inside the film taking into account k-factors for Kα X-rays preset values. The ED experiments were performed in microdiffraction mode for the cross-section sample using a slightly convergent nanobeam in order to record patterns either on the film or on the substrate. The Selected Area Electron Diffraction (SAED) mode was applied for the plan-view sample. The analyses done on each sample, cross-section and plan-view, allowed to get patterns scattered in different zones of the reciprocal space. This is essential to reach the zone axes of highest symmetry as well as to obtain the different reflection conditions of the structure to be identified. Two atomic models were created from the obtained experimental results and crystal data found in the literature. The models and the corresponding crystallography files were done with VESTA **[28]** then exported to the TEM software package JEMS for ED simulations **[29]**. The 2-beams dynamical approach was used for the calculations. We started the simulations with a sample thickness of 100 nm then adjusted this parameter in order to fit with experiments.

The APT technique allowed to analyze the atomic distribution of the annealed sample in three dimensions. A specific specimen preparation in tip shape was realized with FIB milling **[30]**. APT analyses were carried out in a LEAP 3000X HR instrument. The specimen temperature was set to 33.5 K, the laser pulsing rate to 200 kHz, and the detection rate kept to 0.002 event/pulse by increasing the applied voltage. The reconstruction was based on the SEM

image obtained at the end of the tip preparation. The IVAS 3.6.8 software was used for the reconstruction, visualization and analyses of the APT data.

3. Results

In Figure 1, up to 4 hours, the only measured peaks correspond to the deposited Ni film. This film is preferentially oriented with (111) planes parallel to the surface but a small peak indicates that some grains are also oriented with (200) planes. After 4 h of annealing at 175°C, the Ni peaks disappear and three new ones appear at 2θ=25.7°, 52.8° and 83.7°. As up to the end of the annealing, no new peak appears and a shift towards higher 2θ values is observed. The presence of this shift is discussed in the next section. Then it can be assumed that only one phase has been formed with consumption of the Ni film.

A bright field image of the cross-section sample was recorded for a substrate orientation in [110] zone axis regarding to the electron beam (Fig. 1b). From this image, the substrate-film interface is relatively flat with a lower roughness than the one observed between the film and the protective TiN layer. The thickness of the formed phase is about 198 ± 1 nm and a homogeneous contrast can be observed. Electron microdiffraction patterns recorded in several areas of the film were identical with the same orientation. A multiple-point EDS profile done starting at the middle of the film up to the top in scanning mode gave an estimation of the atomic composition (Fig. 1c). The result was 58% at. Ni, 22% at. In and 20% at. As with an error percentage of ± 2%, that is in agreement with a Ni_3InAs stoichiometry. However, the Cliff-Lorimer approach has limitations because of the preset values of the K-factors, this can be optimized using standard of composition. The absorption of X-rays within the specimen can also generate errors in the quantification. The nanostructure (phase/InAs) was then also analyzed by APT in order to determine the atomic distribution in three dimensions on both sides of the film-substrate interface and measure the precise chemical composition. Figure 2a

shows the $40 \times 40 \times 95$ nm^3 reconstructed volume in which Ni, As and In atoms are shown using green, red and blue dots, respectively. The APT volume indicates a homogenous distribution of all atoms confirming the presence of a single phase. The composition was deduced from the mass spectrum available as support information. Despite the absence of overlapping of elementary peaks, we observed As_2^{2+} and As^+ ions occupy the same peak position at 75 Da. Then, we have checked the composition taking into account either single or multiple events, which gave no significant difference. Assigning As^+ to the mentioned peak gave the best fit with the known stoichiometry of the substrate (50% at. In and 50% at. As). Figure 2b shows a one-dimensional composition profile calculated in a cylindrical region of the sample perpendicular to the interface, having a diameter of 20 nm. The cylindrical region is represented in figure 2a. The chemical composition averaged over the nickelide layer is 60% at. Ni, 21% at. As and 19.0% at. In corresponding to $Ni_{3.0}In_{0.96}As_{1.04}$. Therefore, the first results can be understood such as the film behaves like a single crystal phase with a strong relationship with the substrate.

ED experiments in microdiffraction (Fig. 3a) and selected area modes (Fig. 3b-e) were performed on the cross-section and plan-view samples respectively in order to obtain patterns scattered in different zones of the reciprocal space. The datasets converged towards the $P6_3/mmc$ hexagonal space group with the unit cell parameters a = b = 4.00 ± 0.10 Å and c = 5.10 ± 0.10 Å. Indeed, the experimental ED patterns of highest symmetry showed the 6-fold [001], 2-fold [100] and 2-fold [210] zone axes (Fig. 3a-c) related to the hexagonal crystal system. The presence of (0k0: $k \neq 3n$) reflections with weak intensities were observed in the [100] (Fig. 3b) and [201] (Fig. 3d) patterns. Then, we could assume there was no specific reflection condition for 0k0 (or h00), all are permitted in the identified hexagonal structure. On the contrary, the weak (00l: l odd) reflections on the [100] ED pattern (Fig. 3b) are actually forbidden owing to the 6_3-screw axis but appear by the well-known phenomenon of

multiple electron diffraction **[31]**. The first results show structural characteristics very similar to the Ni_3GaAs ($B8_{\sim 1.5}$) phase. This phase is closely related to γ-Ni_3Ga_2 whose structure is intermediate between the ones of NiAs ($B8_1$) and Ni_2In ($B8_2$) **[32]**. In $B8_{\sim 1.5}$, an additional Ni atom is randomly distributed on one of two equivalent interstitial sites. In $B8_2$, both of these sites are occupied by Ni atoms whereas in $B8_1$, they are both vacant. ED patterns were simulated using the space group and unit cell parameters found experimentally. The coordinates of the Ni, In and As asymmetric atoms were set with the Ni_3GaAs ($B8_{\sim 1.5}$) arrangement which is defined with the same stoichiometry than the one we found experimentally. Ni_1 was set at (0, 0, 0) with full occupation; Ni_2 (1/3, 2/3, 1/4) and Ni_3 (1/3, 2/3, 3/4) each one randomly distributed with an occupation of 40%; In (1/3, 2/3, 1/4) and As (2/3, 1/3, 3/4) each one randomly distributed with an occupation of 60% (Fig. 4a). The results show a good agreement with the experimental patterns concerning the position as well as the intensity ratios of the reflections (Fig. 3f-j). Another arrangement defined with the Ni_3InAs stoichiometry was studied using vacancies sharing interstitial sites with In and As atoms: Ni was set at (0, 0, 0); In (1/3, 2/3, ¼) and As (1/3, 2/3, ¾) were randomly distributed with an occupation of 33.33% (Fig. 4b). The reflection intensities calculated from this structure (fig. 3k-o) are not relevant as compared with the ones obtained for the previous model. Especially, the (010) and (002) reflections were respectively found with higher and lower intensity as compared with experiments. The structure of the obtained nickelide phase seems to correspond to a disordered model with Ni atoms randomly distributed in the interstitial sites of the hexagonal lattice. The crystallography files of each model are available as supplement information.

The identification of the structure and unit-cell parameters of the Ni_3InAs phase allowed to index the corresponding X-Ray diffraction peaks that appeared during the diffusive reaction (Fig. 1a). The peaks located at the 2θ values of 25.7°, 52.8° and 83.7° are respectively

attributed to the (100), (200) and (300) diffracted planes of the identified hexagonal structure. This texture confirms the strong relationship with the substrate that explains the absence of any other reflexion. The presence of (100) and (200) peaks observed by XRD confirms that there is no specific reflection condition for h00 (or 0k0).

An experimental HRTEM image (Fig. 5a) was recorded using the cross-section sample for a [110] zone axis of the substrate regarding to the electron beam. The power spectra calculated on both sides of the interface highlight the zone axes relationship between the substrate (s) and the film (f), namely $[110]_s//[001]_f$, as well as the orientations of atomic planes, namely $(220)_s//(-120)_f$ and $(002)_s//(100)_f$. Knowing the lattice geometries of the substrate and the film, the epitaxy $[001]_s//[210]_f$ was deduced. These results are in accordance with the fact that the film is highly textured as shown by the X-Ray diagram. Indeed, the following relationship $(004)_s//(100)_f$ has been found and is compatible with the one given by the HRTEM result, namely $(002)_s//(100)_f$. We can noticed that $(002)_s$ reflection was detected in ED but not in XRD. This reflection forbidden by the F-43m space group, appears in ED by the multiple diffraction phenomenon, as mentioned previously.

4. Discussion

The EDS and APT analyses performed on the nickelide phase gave an atomic composition in agreement with Ni_3InAs. The thickness of the formed phase after reaction could provide information on the obtained stoichiometry since both are related to the volumetric ratio $V_{NixInAs}/V_{Ni}$; $V_{NixInAs}$ is the unitary volume of Ni_xInAs, V_{Ni} the atomic volume of Ni and x the number of Ni atoms in the nickelide phase. The method had already been used in the case of Ni_xGaAs **[33]**. It is based on the hypothesis that Ni is the diffusing specie into the formed phase to react at the interface with InAs. Once it has reacted, there is no Ni diffusion into InAs, as it has been checked during the APT analysis (Fig. 2b). All Ni atoms have been used to form the nickelide phase. By analogy with the Ni/GaAs system, two

cases were considered, Ni_3InAs and Ni_2InAs. The thickness of the Ni_3InAs phase should increase by a factor of two relatively to the thickness of the consumed Ni ($V_{NixInAs}/V_{Ni} = 2$) whereas it should be of three for Ni_2InAs, assuming similar unit cell parameters for each stoichiometry. The thickness measurement deduced from the cross-section TEM image gives 198 ± 1nm so the volumetric ratio of Ni_3InAs is verified in this case.

Concerning the structure, computational methods by Density Functional Theory (DFT) **[20]** had predicted five crystal systems for the Ni_3InAs nickelide phase. The Ab-Initio Random Structure Searching (AIRSS) approach reported the five lowest-energy for the Pmmn, Pbcm, $P2_1/m$, Cmcm and R-3 space groups that were compared to the limited information of structure available in the literature for Ni_3InAs. Cmcm was found as a higher-energy metastable structure and in agreement with unit-cell parameters found from only one HRTEM image of ref. **[13]**. The crystal parameters proposed in the present study as well as the disordered arrangement of Ni, In and As atoms in interstitial sites could be used to calculate the formation energy of the structure and to study the stability of the energy states with temperature.

In the Ga-Ni-As ternary system, different studies were done on a NiAs - $Ni_{3.55}Ga_{1.5}As_{0.5}$ composition line. The results showed the occurrence of two fully disordered structures crystallizing in a NiAs-type hexagonal symmetry, as well as three ordered structures forming hexagonal superlattices derivative from the NiAs-type structure **[23, 34]**. In particular, the ($a\sqrt{3}$, 3c) one was found in a $Ni_3Ga_{0.75}As_{1.25}$-Ni_3GaAs composition range. The cooling mode could explain the occurrence of the superlattice obtained after a slow process, or of a single disordered phase after quenching in ice water. The same ordered structure was observed for an identical atomic composition in the quite similar Ni-Al-As phase diagram **[35]**. In our case, the Ni_3InAs structure was formed after 4 h at a low temperature of 175°C then kept during 65h. The heating was then switched off without a controlled cooling ramp. We can assume

that a transition from a disordered to an ordered arrangement could not take place due to the low heating temperature and the absence of controlled cooling ramp. Another hexagonal superlattice (2a, 4c) was found in the $Ni_3Ga_{1.5}As_{0.5}$-Ni_3Ga_2, which would be not a ternary phase but an extension of the monoclinic (C2/m) γ'-$Ni_{13}Ga_9$ phase. The superlattice is described in an orthogonal projection of the monoclinic γ'-$Ni_{13}Ga_9$ unit cell. This representation can be seen like a hexagonal cell in which the atomic arrangements do not translate correctly. The third hexagonal superlattice (3a, 2c) has the atomic composition : 54%Ni; 8%Ga; 32%As. The three ordered ternary phases with hexagonal superlattices were unambiguously identified by TEM **[36]**. In our case, the ED experiments by TEM clearly converge towards a B8 structure of hexagonal $P6_3/mmc$ space group. No additional reflection or column of reflections that could justify the presence of an ordered superslattice was found in the several ED patterns recorded in scattered areas of the reciprocal space. Our results show the formation of the Ni_3InAs hexagonal structure in epitaxy as one and only phase after the reactive diffusion between a Ni thin film and an InAs substrate.

In the diffusion couples of Ni/GaAs and Ni/InAs systems, the first phase to form has the composition corresponding to Ni_3GaAs and Ni_3InAs, respectively **[37]**. The presence of only one phase suggests that its formation kinetics must be very fast. Recently, it has been shown by experimental and theoretical investigations that the first formed phase is mainly piloted by atomic kinetics in the phases and not by thermodynamic phase equilibrium or phase nucleation **[38]**. Thus, the first phase that forms during the reactive diffusion is the one exhibiting the highest value in growth kinetics. Indeed, our APT results have shown that the proportions of In and As in the Ni_3InAs phase are equivalent regarding to the InAs substrate. This implies that Ni is the diffusing specie in the phase during its growth and the reaction occurs only at the film-substrate interface in agreement with the literature on GaAs and InGaAs **[33]**. The fast Ni diffusion has been explained by a mechanism using double

tetrahedral interstitial sites and vacancies of the Ni sublattice for the B8 hexagonal structure **[39]**. The shift of the (h00) planes observed from XRD experiments may be explained by the evolution of the local thermodynamic equilibrium when the Ni film is fully consumed. Indeed, this shift matches with the end of the consumption of the Ni film. Before the end of the Ni consumption, Ni_3InAs exhibits a composition gradient based on two thermodynamic equilibria (Ni/Ni_3InAs and Ni_3InAs/InAs) between the Ni film and the InAs substrate. When the Ni film is fully consumed, only one local equilibrium between Ni_3InAs and InAs remains, leading to a composition homogenization of Ni_3InAs. This homogenization induces a gap on the interplanar spacing of the (h00) planes. This behavior is similar to the one recently observed in the Ni/GaAs system because Ni_3GaAs phase also yields a large domain of homogeneity in the composition **[40]**.

In the present study, the texture determined by TEM, $[110]_s//[001]_f$, $(220)_s//(-120)_f$ and $(002)_s//(100)_f$ showed a major difference as compared with the one found for the Ni_3GaAs/GaAs system, $[1\text{-}10]_s//[110]_f$ and $(201)_s//(1\text{-}11)_f$ **[40].** The atomic size effects and thus the unit-cell parameters could explain in part the modification of texture and interface energy. Indeed, the growth of a film in epitaxy on a monocrystalline substrate is possible if this configuration lead to minimize the energy of the system. We consider that the energy should be minimized if the misfit between the lattice parameters of the phase and the substrate was also minimized (decreasing the interface energy and the strain energy in the phase). The lattice parameters of Ni_3InAs (a=4.00 Å and c=5.10 Å) are larger than Ni_3GaAs ones (3.87 Å and c=5.03 Å) **[32]** in relation with atomic size effect; the indium atoms (Ra=155 pm) are larger than gallium (Ra=130 pm) ones. This effect can be clearly observed between InAs (a=6.05 Å) and GaAs (a=5.65 Å) substrates **[41]**. Moreover, the lattice misfit values have been compared for each system considering both epitaxy relationships (Table). This could thus explain the texture difference between the Ni_3InAs/InAs and Ni_3GaAs/GaAs systems.

5. Conclusion

In summary, a Ni_3InAs phase was identified by TEM and APT techniques in a nanoscale thin film on InAs substrate. This phase was formed in epitaxy by a solid-state reaction between a 100 nm Ni film and an InAs (001) substrate at relatively low temperature (175°C). Especially, the $P6_3/mmc$ SG was precisely identified and the results show characteristics very similar to the disordered Ni_3GaAs ($B8_{\sim 1.5}$). Compared with the $Ni_3GaAs/GaAs$ system, the major difference concerns the lattice parameters and epitaxy relationship that can be assigned to differences in atomic sizes and lattice mismatch values. The relatively abrupt interface with self-aligned contacts obtained from a magnetron sputtering deposition at low temperature suggest their use in the field of III-V based transistors.

The data that support the findings of this study are available within the supplementary material.

This work is supported by PHC Tassili number 17MDU994 between Algerian and French Ministries of Higher Education.

References

[1] Ho, J.C., Yerushalmi, R., Jacobson, Z.A., Fan, Z., Alley, R.L., & Javey, A., Nature Materials, 2008, 7, 62–67

[2] Javey, A., Guo, J., Wang, Q., Lundstrom M., & Dai H., Nature, 2003, 424, 654–657

[3] Larson, J.M., & Snyder, J.P., IEEE Transactions on Electron Devices, 2006, 53, 5, 1048-1058

[4] Hu, Y., Xiang, J., Liang, G., Yan, H., & Lieber, C.M., Nano Letters, 2008, 8, 3, 925-930

[5] del Alamo, Jesus A., Nature, 2011, 479, 317–323

[6] Lind, E., Persson, A.I., Samuelson L., & Wernersson L.-E., Nano Letters, 2006, 6, 9, 1842-1846

[7] Dayeh, S.A., Yu, E.T., & Wang, D., J. Phys. Chem. C, 2007, 111, 36, 13331-13336

[8] Ford A.C., Ho, J.C., Fan Z., Ergen, O., Altoe, V., Aloni, S., Razavi, H., & Javey A., Nano Research, 2008, 1, 32-39

[9] Jiang, X., Xiong, Q., Nam, S., Qian, F., Li, Y., & Lieber, C.M., Nano Letters, 2007, 10, 3214-3218

[10] Jan C.H., Swenson, D. & Chang Y.A., Journal of Applied Physics, 1990, 68, 6458

[11] Murakami, M., Price, W.H., Greiner, J.H., & Feder J.D., Journal of Applied Physics, 1989, 65, 3546

[12] Han, C.C., Wang, X.Z., Wang, L.C., Marshall, E.D., & Lau S.S., Journal of Applied Physics, 1990, 68, 5714

[13] Oxland, R., Chang, S.W., Li, X., Wang, S.W., Radhakrishnan, G., Priyantha, W., van Dal, M.J.H., Hsieh, C.H., Vellianitis, G., Doornbos, G., Bhuwalka, K., Duriez, B., Thayne, I., Droopad, R., Passlack, M., Diaz, C.H., & Sun, Y.C., IEEE Electron Device Letters, 2012, 33, 4, 501-503

[14] Chueh, Y.-L., Ford, A.C., Ho, J.C., Jacobson, Z.A., Fan, Z., Chen, C.-Y., Chou, L.-J., & Javey, A., Nano Letters, 2008, 8, 12, 4528-4533

[15] Beyers, R., Kim K.B., & Sinclair R., Journal of Applied Physics, 1987, 61, 2195

[16] Sands, T., JOM, 1986, 38, 10, 31-33

[17] Tsai, C.T., & Williams, R.S., Journal of Materials Research, 1986, 1, 820

[18] Lin, J.-C., Hsieh, K.-C., Schulz, K. J., & Chang, Y. A., Journal of Materials Research, 1988, 3, 1, 148-163

[19] Shiau F.-Y. & Chang, Y.A., Materials Research Society Symposium, 1989, 148, 29

[20] Schusteritsch, G., Hepplestone, S.P., & Pickard C.J., Physical Review B, 2015, 92, 054105

[21] Swenson, D., & Chang, Y.A., Materials Science and Engineering, 1996, 39, 3, 232-240

[22] Chen, S.-Y., Wang, C.-Y., Ford, A.C., Chou, J.-C., Wang, Y.-C., Wang F.-Y., Ho, J.C., Wang, H.-C., Javey, A., Gan, J.-Y., Chen, L.-J., & Chueh, Y.-L., Physical Chemistry Chemical Physics, 2013, 8, 2654

[23] Ingerly, D.B., Swenson, D., Jan, C.-H. & Chang, Y.A., Journal of Applied Physics, 1996, 80, 1, 543-550

[24] De Schutter, B., De Keyser, K., Lavoie, C., & Detavernier, C., Applied Physics Reviews, 2016, 3, 031302

[25] Giannuzzi, L.A., Drown J.L., Brown S.R., Irwin R.B., & Stevie F.A., Microscopy Research and Technique, 1998, 41, 4, 285-290

[26] Patout, L., Hallaoui, A., Neisius, T., Campos, A. P. C., Dominici, C., Alfonso, A., & Charaï, A., Journal of Applied Crystallography, 2018, 51, 344-350

[27] Patout, L., Alfonso, & C., Charaï, A., Materialia, 2020, 9, 100545

[28] Momma, K., & Izumi, F., Journal of Applied Crystallography, 2011, 44, 1272-1276

[29] Stadelmann, P. A., Ultramicroscopy, 1987, 21, 2, 131–145

[30] Panciera, F., Hoummada, K., Gregoire, M., Juhel, M., Lorut, F., Bicais N. & Mangelinck D, Microelectronic Engineering, 2013, 107, 167

[31] Morniroli, J.P. & Steeds, J.W., Ultramicroscopy, 1992, 45, 2, 219-239

[32] Zheng, X.-Y., Lin, J.-C., Swenson, D., Hsieh, K.-C., & Chang, Y., Materials Science and Engineering B, 1989, 5, 63-72

[33] Perrin, C., Ghegin, E., Zhiou, S., Nemouchi, F., Rodriguez, P., Gergaud, P., Maugis, P., Mangelinck, D., & Hoummada, K., Applied Physics Letters, 2016, 109, 131902

[34] Guérin R. & Guivarc'h A., Journal of Applied Physics, 1996, 80, 543

[35] D. Deputier, R. Guérin, Y. Ballini, & A. Guivarc'h, Journal of Alloys and Compounds, 1995, 217, 13

[36] A. Poudouloulec, B. Guenais, A. Guivarc'h, J. Caulet, & R. Guérin, Journal of Applied Physics, 1991, 70, 7613

[37] Sutopo, International Journal of Engineering & Technology IJET-IJENS, 2011, 11, 5, 28-33

[38] Toinin, J.P., Hoummada, K., Bertoglio, M. & Portavoce, A., Scripta Materialia, 2016, 122, 22-25

[39] Hähnel, R., Miekele, W., Wever, H., Phys. Status solidi A 97, 1986, 181-190

[40] Rabhi, S., Perrin-Pellegrino, C., Zhiou, S., Benoudia, M.C., Texier, M., & Hoummada, K., Scripta Materialia, 2017, 141, 28-31

[41] Grundmann, M., Stier, O., & Bimberg, D., Physical Review B, 1995, 52, 16, 11969

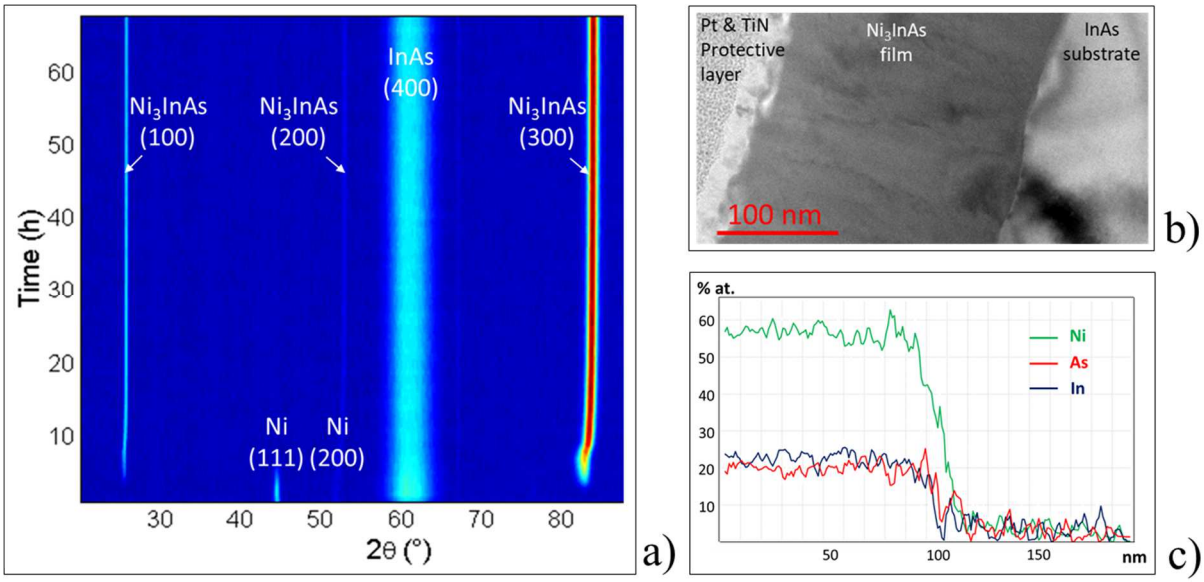

Figure 1: In situ XRD diagram recorded during the diffusive reaction between the Ni deposited film and the InAs substrate (a). Bright field TEM image of the cross-section sample (b). EDS profile line highlighting the Ni_3InAs stoichiometry of the formed phase (c).

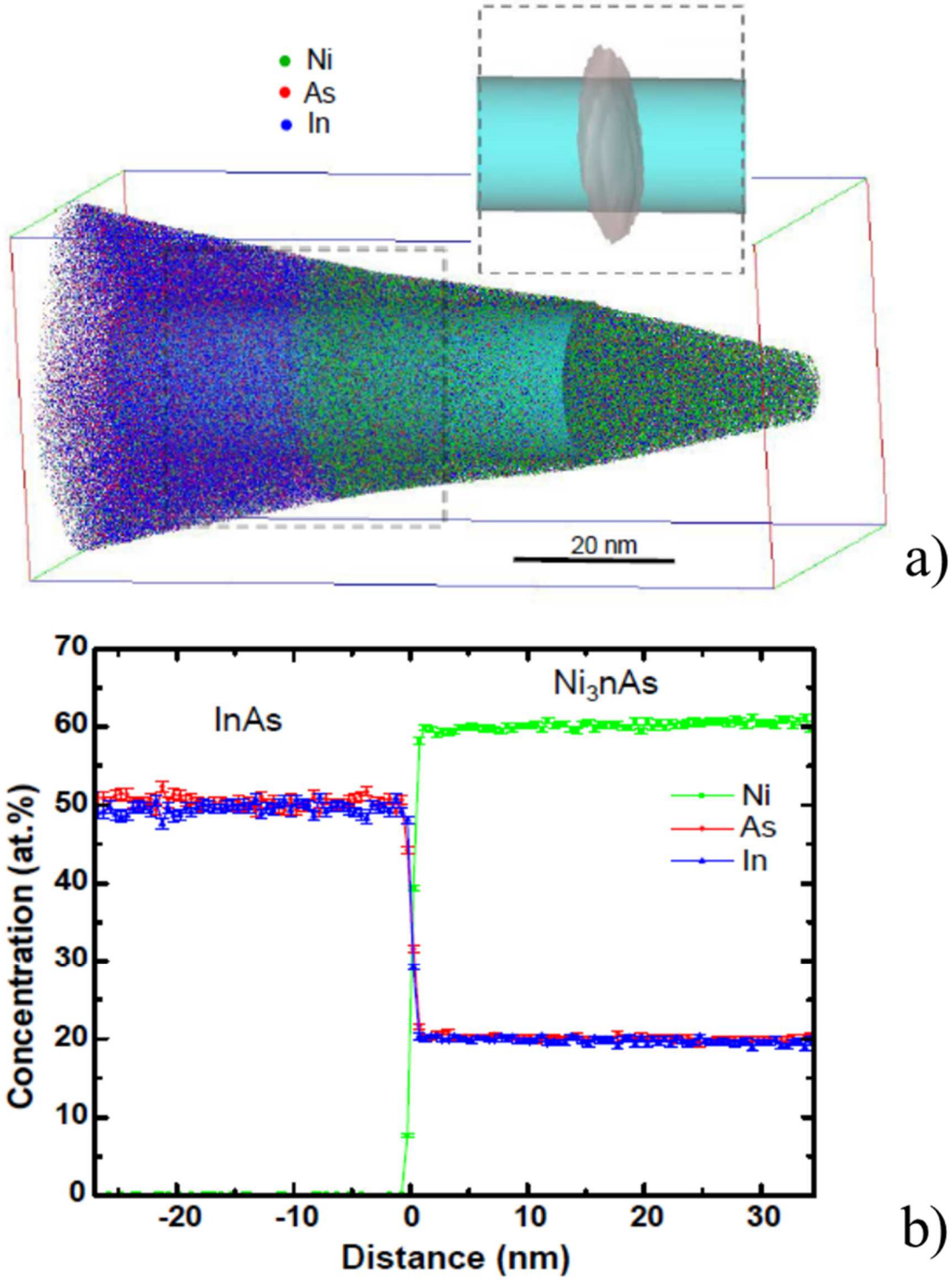

Figure 2: APT analysis performed on the sample after annealing at 175°C for 69h. 3D reconstructed volume showing the As (red dots), Ni (green dots) and In atoms (blue dots) (a). One-dimensional composition profiles measured from the APT volume in the perpendicular direction of the surface within a 20 nm diameter cylindrical volume (b). The isosurface of 30% at. Ni used to define the phase-substrate interface is represented in the inset.

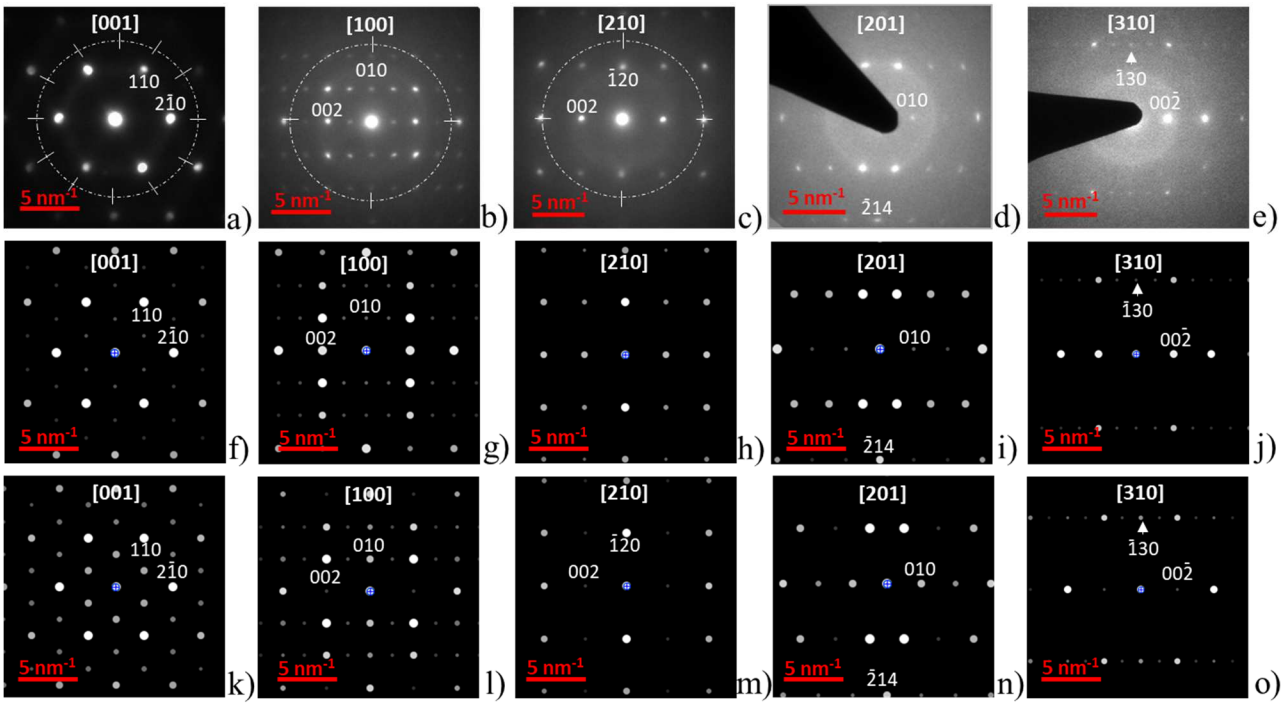

Figure 3: Experimental ED patterns (a-e) recorded on the Ni_3InAs film. (a) was recorded by microdiffraction on the cross-section sample. (b-e) were recorded by selected area on the plan-view sample. The white circles in hashed line highlight the 6-fold [001] (a), 2-fold [100] (b) and 2-fold [210] (c) zone axes of the hexagonal structure. Simulated patterns of the disordered structures: additional Ni atoms are randomly distributed on the interstitial sites (f-j); In and As atoms share their interstitial sites with vacancies (k-o).

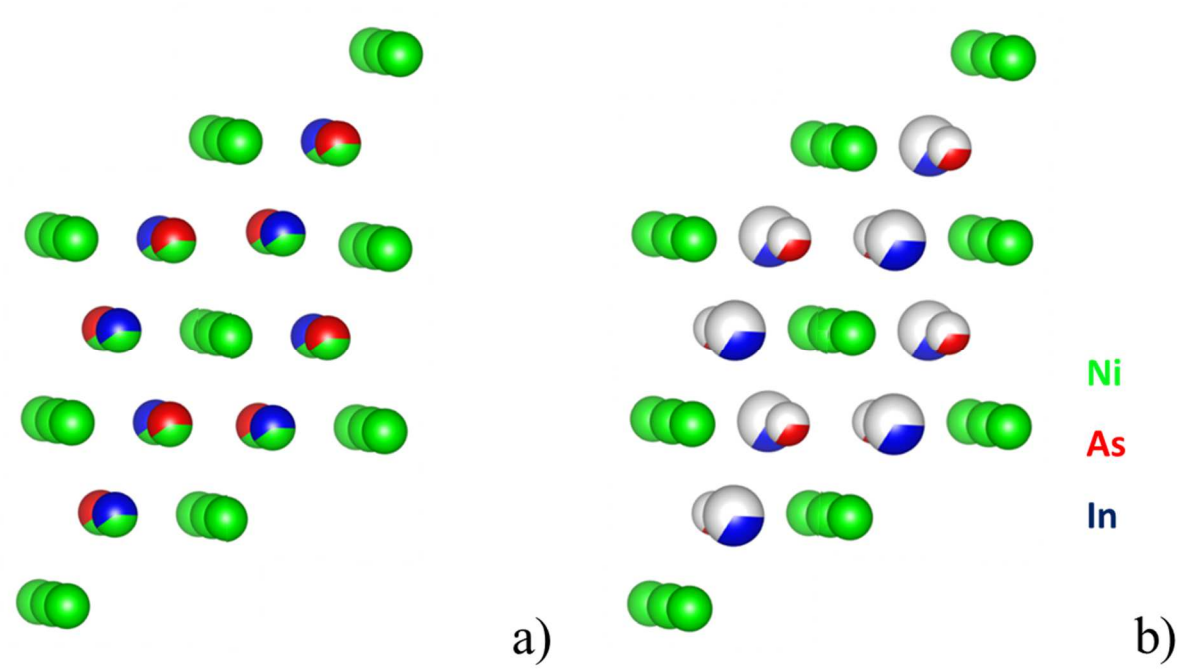

Figure 4: Representation of the models used for ED simulations. Ni atoms are randomly distributed in interstitial sites (a). Vacancies are randomly distributed in interstitial sites (b).

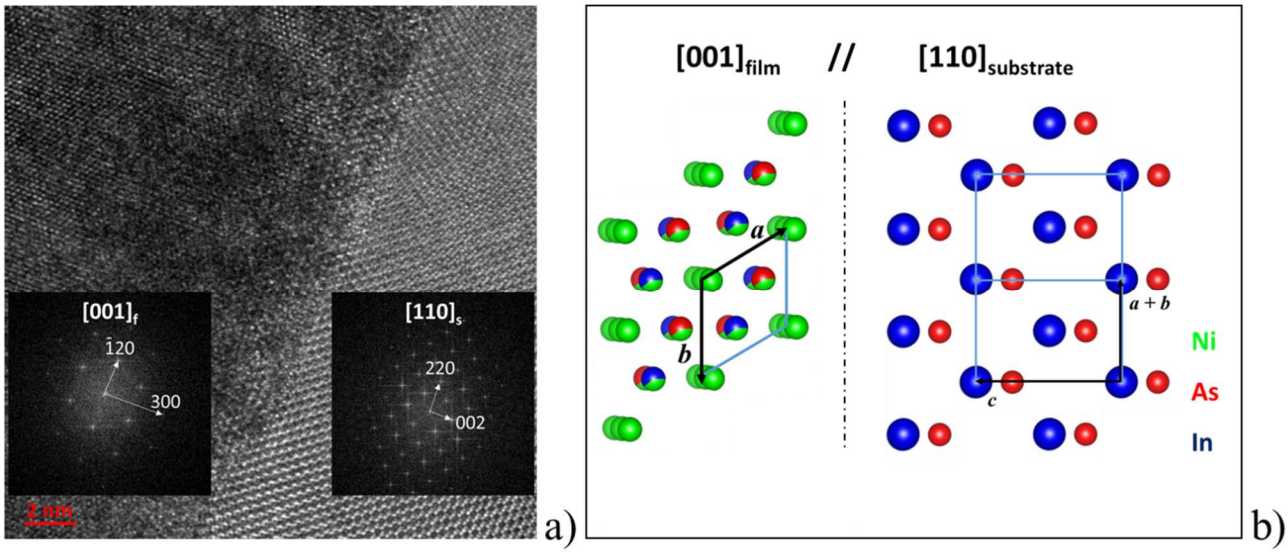

Figure 5: Experimental HRTEM image of the cross-section sample (a) and the atomic representation (b) highlighting the orientation relation between the Ni_3InAs film and the InAs substrate.

Epitaxy relationship	(2-20)s//(-120)f and [110]s//[001]f			(201)s//(1-11)f and [1-10]s//[110]f		
Interreticular distances (nm)	d(110)s	d(002)f	Mismatch between 6 planes of substrate and 5 planes of film	d(220)s	d(-112)f	Mismatch between 6 planes of substrate and 5 planes of film
Ni3InAs / InAs	0.2139	0.2550	**0.7%**	0.2139	0.2054	-4.0%
Ni3GaAs / GaAs	0.1998	0.2515	4.9%	0.1998	0.2012	**0.7%**

Table: Comparison of the lattice mismatches of both systems (Ni_3GaAs and Ni_3InAs) and epitaxy relationships.

Support information

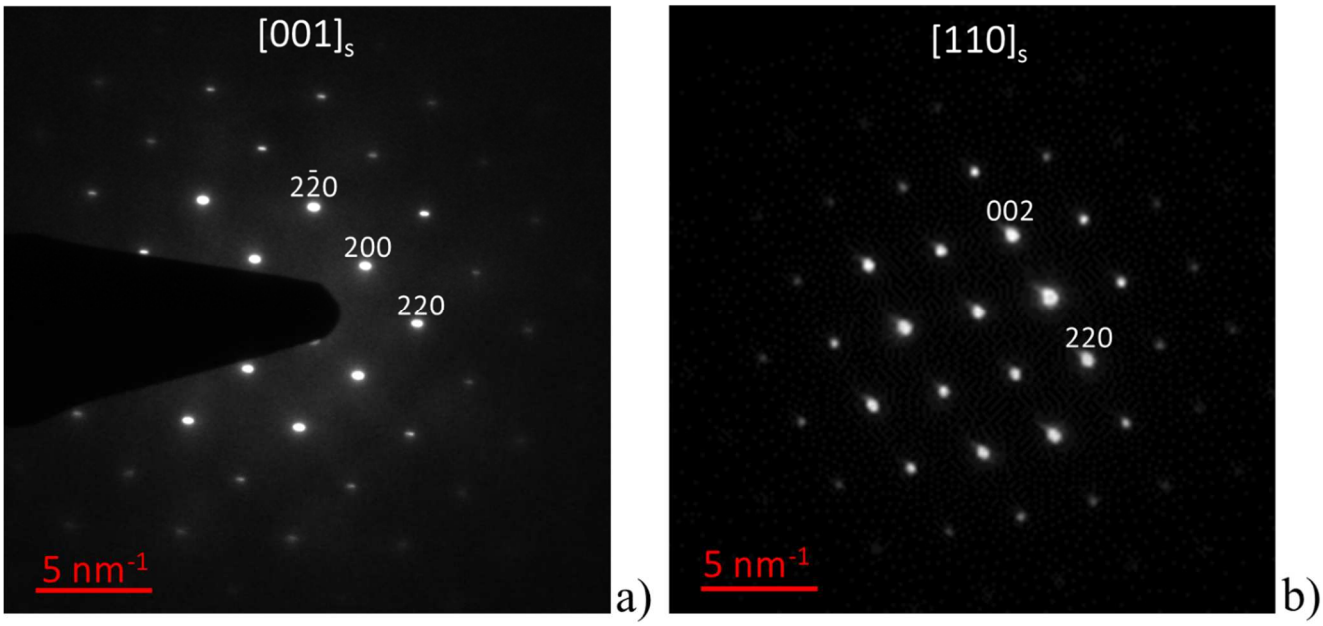

Figure: ED patterns of the substrate obtained in SAED a) and microdiffraction b) modes in the plan-view and cross-section samples respectively.

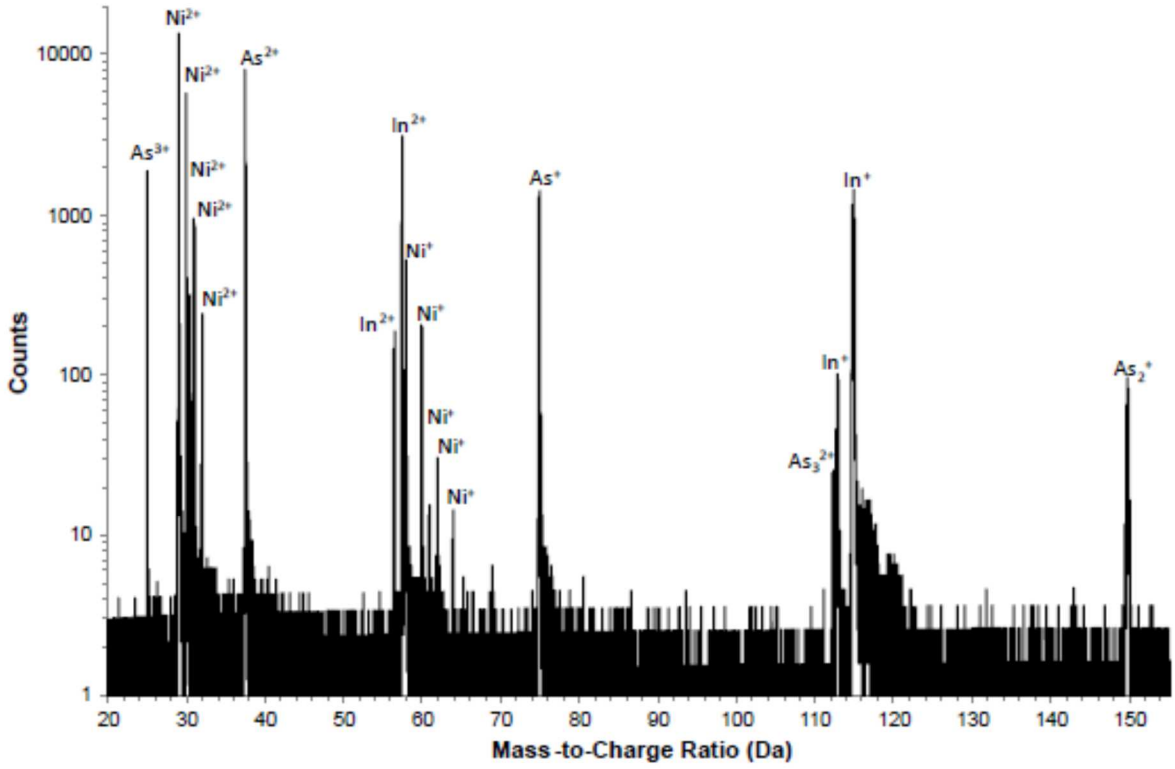

Figure: Mass spectrum obtained in the Ni_3InAs phase.

Ni3InAs-Ni-interstitial.cif

Ni3InAs-vacancies-interstitial.cif

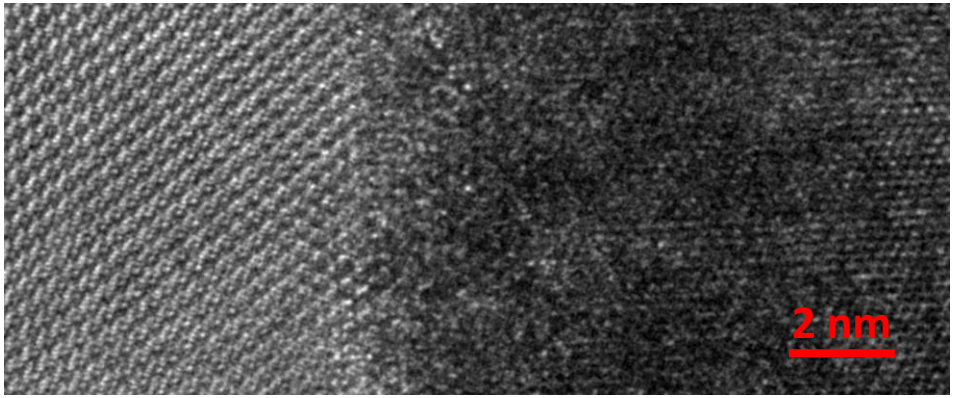
2 nm

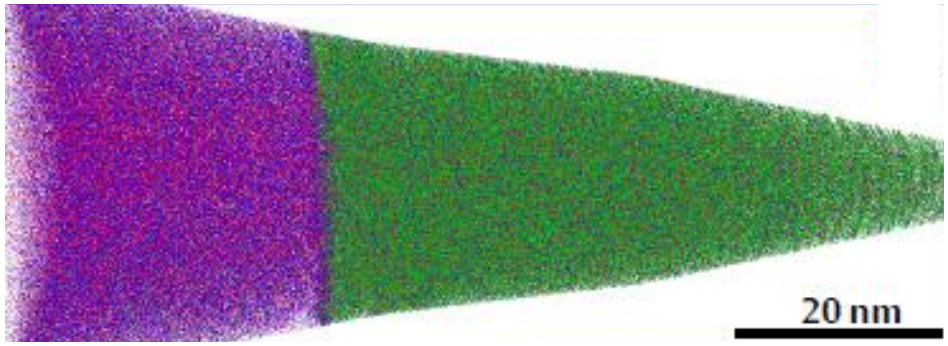
20 nm

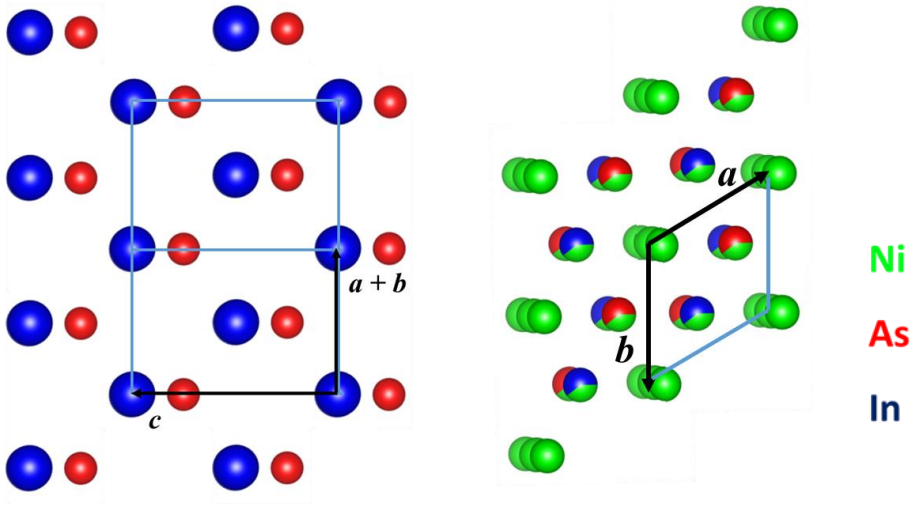
a + b
c
a
b
Ni
As
In